


Carbon nanofiber-based $\text{CuSn}(\text{OH})_6$ and CuSnO_3 composites for NO_2 gas sensors and supercapacitors

Anton V. Loginov ^{*} , Alexander I. Aparnev , Oksana N. Novgorodtseva 
Alexander G. Bannov 

Faculty of Mechanical Engineering and Technologies, Novosibirsk State Technical University ,
Novosibirsk 630073, Russia

* Corresponding author: loginov@corp.nstu.ru



Abstract

Copper hydroxystannate, $\text{CuSn}(\text{OH})_6$, was obtained via a hydrothermal method from a mixture of solutions of copper(II) chloride and sodium stannate with the addition of sodium hydroxide solution until pH 10. The phase compositions of the hydrothermal synthesis and the thermal decomposition products were studied using thermal analysis, X-ray diffraction, scanning electron microscopy, and FTIR spectroscopy. It was established that at a synthesis temperature of 180 °C, a single-phase perovskite-like copper hydroxystannate is formed, with particles having cubic shapes measuring 35–38 nm (according to Scherrer's equation). It was shown that the reaction of the CuSnO_3 /modified CNFs composite with NO_2 at room temperature results in a 32% response at 2 ppm, whereas the response of the $\text{CuSn}(\text{OH})_6$ /modified CNFs composite under the same conditions is 19%. The CuSnO_3 /modified CNF composite exhibits the best electrochemical characteristics compared to the $\text{CuSn}(\text{OH})_6$ /modified CNF composite for use in supercapacitors. The composite material CuSnO_3 /modified CNFs demonstrated its applicability as an electrode material in supercapacitors, showing a specific capacitance of 288 F/g at a scan rate of 2 mV/s, compared to the $\text{CuSn}(\text{OH})_6$ /modified CNFs (135 F/g). It was established that the specific capacitance of composites based on CNFs significantly exceeds that of single-phase copper stannates (14 and 6 F/g, respectively).

Key findings

- As a result of hydrothermal synthesis, a single-phase perovskite-like copper hydroxostannate $\text{CuSn}(\text{OH})_6$ is formed, which upon thermolysis above 300 °C yields amorphous copper stannate.
- The use of modified CNFs in composites based on $\text{CuSn}(\text{OH})_6$ and CuSnO_3 enhances NO_2 detection.
- The CuSnO_3 /modified CNFs composite exhibits the best electrochemical characteristics compared to the $\text{CuSn}(\text{OH})_6$ /modified CNF composite for use in supercapacitors.

© 2025, the Authors. This article is published in open access under the terms and conditions of the Creative Commons Attribution (CC BY) license (<http://creativecommons.org/licenses/by/4.0/>).

1. Introduction

Perovskite-type hexahydroxystannates of *d* metals (such as Cu, Zn, Cd, Mn, Fe, Co, Ni) and alkaline earth metals (for example, Mg, Ca, Sr, Ba) with the general formula $\text{MSn}(\text{OH})_6$ attract significant attention due to their wide range of potential applications in various fields, including the development of gas-sensitive sensor elements [1–3], anode materials for batteries and supercapacitors, autonomous energy devices for energy storage and conversion [4–11], and catalysis and photocatalysis [12–19]. Additionally,

mixed hydroxides serve as precursors for the synthesis of metastannates (MSnO_3) and ortistanates (M_2SnO_4). These compounds are characterized by special chemical properties, unique crystal structures, and increased thermal stability. The synthesis of hexahydroxystannates and stannates of metals is carried out using sol-gel methods, precipitation techniques, and hydrothermal synthesis [3,12,20–26].

Recent studies have shown that perovskite-based composites possess excellent electrochemical properties, making them promising for use as sensing materials in sensors

Accompanying information

Article history

Received: 10.10.25

Revised: 12.11.25

Accepted: 19.11.25

Available online: 27.11.25

Keywords

copper hydroxostannate; copper stannate; hydrothermal method; carbon nanofibers; nitrogen dioxide; sensor; composite

Funding

The work was carried out in accordance with the state task of the Ministry of Education and Science of Russia (project FSUN-2023-0008).

Supplementary information

Transparent peer review:  READ

Sustainable Development Goals



and electrodes of supercapacitors. Over the past few years, several new materials have been developed aimed at increasing specific capacity of the latter. In the energy storage devices, supercapacitors are gaining increasing attention [27–29] due to characteristics such as high specific capacitance, increased power density, prolonged operational lifespan, affordable cost, environmental and human safety, and rapid charge-discharge processes. For example, in [30], it was found that the specific capacitance of composites correlates with their specific surface area. Highly porous hydrothermally synthesized nanocomposites based on NiSnO_3 and graphene with a surface area of $162 \text{ m}^2/\text{g}$ demonstrated a specific capacitance of 891 F/g , whereas pure NiSnO_3 nanoparticles ($S = 101 \text{ m}^2/\text{g}$) had a specific capacitance of 570 F/g . In another study [31], the nanocomposite $\text{FeSnO}_3/\text{reduced graphene oxide}$ also showed a high specific capacity (1342 F/g). Wang G. et al. [32], using a simple co-precipitation method, obtained composite materials based on MnSn(OH)_6 and established that the total specific capacitance strongly depends on the crystallinity of the nanoparticles, where materials with lower crystallinity exhibited a maximum value of 31.2 F/g (an increase of over 300% compared to bulk manganese hydroxostannate nanoparticles). Furthermore, the authors experimentally demonstrated that higher crystallinity and larger crystallite size lead to increased diffusion resistance and, consequently, impact the electrochemical reaction. The hydrothermal method was used for the synthesis of nickel-doped cadmium stannate ($\text{Cd}_{1-x}\text{Ni}_x\text{SnO}_3$) [33]. The resulting composite material demonstrated improved characteristics, notably a higher specific capacity. The authors experimentally established that the specific capacitance of the modified composite reaches 557.6 F/g at a current of 0.2 A/g , significantly exceeding the corresponding value for undoped cadmium stannate. In [9], NiSn(OH)_6 hexahydroxide nanoparticles were synthesized by co-precipitation, showing a maximum specific capacity of 607 F/g . The authors also noted that a composite with activated carbon exhibits high energy density and high power density, that along with excellent cyclic stability, make it an ideal material for supercapacitors.

Among numerous hydroxystannates and stannates, mixed hydroxides of copper and tin(IV), as well as copper stannate, are used in various catalytic processes and as anode materials for batteries [34–36]. The method used to synthesize these compounds influences their structure and morphology, which, in turn, determines their areas of application [37–41]. To improve the electrochemical properties of metal stannates, researchers are actively developing composites that incorporate various additives, such as carbon materials [9,31–33,42].

In this study, we investigated the possibility of using CuSn(OH)_6 and its thermolysis product (CuSnO_3) as materials for the fabrication of gas sensor sensing elements and electrodes intended for energy storage devices.

2. Materials and Methods

2.1. Materials

In the work, the following substances were used as starting reagents: $\text{CuCl}_2 \cdot 2\text{H}_2\text{O}$ (GOST 4108-72 “Cupric chloride 2-water”, pure, «Odhim» LLC, Moscow, Russia), $\text{Na}_2\text{SnO}_3 \cdot 3\text{H}_2\text{O}$ (metastannate 3-water, TU 6-09-1506-76, pure, LLC “Spektr-chem SPb”, St. Petersburg, Russia), and NaOH (GOST 4328-77 “Sodium hydroxide”, chemical pure, LLC “Khimprom, Perm Region, Russia,). The purity of the reagents is indicated in the certificates provided by the product suppliers. For preparing a 1 M solution of NaOH , bidistilled water obtained from the VE-2 purification unit was used. All the reagents were used in the form in which they were received, without additional purification.

2.2. Synthesis and characterization of CuSn(OH)_6

Copper hydroxystannate CuSn(OH)_6 was synthesized using a hydrothermal method as follows. First, 0.8525 g (5 mmol) of $\text{CuCl}_2 \cdot 2\text{H}_2\text{O}$ was dissolved in 50 mL of bidistilled water, and to the resulting solution a suspension of 1.3337 g (5 mmol) of $\text{Na}_2\text{SnO}_3 \cdot 3\text{H}_2\text{O}$ was added with vigorous stirring. The obtained mixture was treated in an ultrasonic homogenizer HX-IID HuxiShiYe with a power of 1000 W for 30 s . Then, while stirring, a 1 M NaOH solution was gradually added, maintaining the pH around 10. The pH was monitored using a laboratory pH meter HI 2221. After vigorous stirring for 20 min , the suspension was transferred to a stainless steel autoclave with a Teflon gasket and heated at $180 \text{ }^\circ\text{C}$ for 16 h . After cooling to room temperature, the pale-green precipitate was filtered using a vacuum pump and washed with distilled water until a negative qualitative reaction for chloride ions (Cl^-) was obtained. The precipitate was then dried in a SNOL 6.7/1300 muffle furnace at $110 \text{ }^\circ\text{C}$ for 4 h (see Figure 1).

The phase composition of the samples were determined by X-ray diffraction (XRD). X-ray diffraction patterns were recorded at room temperature using a Bruker D8 Advance diffractometer with $\text{Cu K}\alpha$ radiation in the 2θ range from 10 to 70° . The phases formed in the system were identified using the Crystallographica Search-Match, Version 2.1 program and the PDF4 database. The average size of coherent scattering domains was estimated from diffraction line broadening in X-ray diffraction patterns using the Scherer formula:

$$d = \frac{k\lambda}{\beta \cos \theta}, \quad (1)$$

where d is the average size of coherent scattering domains (\AA), λ is the X-ray wavelength (1.54051 \AA), β is the full width at half maximum of the diffraction peak (rad.), θ is the diffraction angle ($^\circ$), and $k = 0.9$.

Thermal analysis (TA) of the dried powders was performed on a NETZSCH Jupiter 449C STA synchronous thermal analyzer coupled to QMS 403C Aëolos (TG-QMS) mass spectrometer in an argon flow at temperatures in the range of $20\text{--}600 \text{ }^\circ\text{C}$ at a heating rate of $10 \text{ C}\cdot\text{min}^{-1}$.

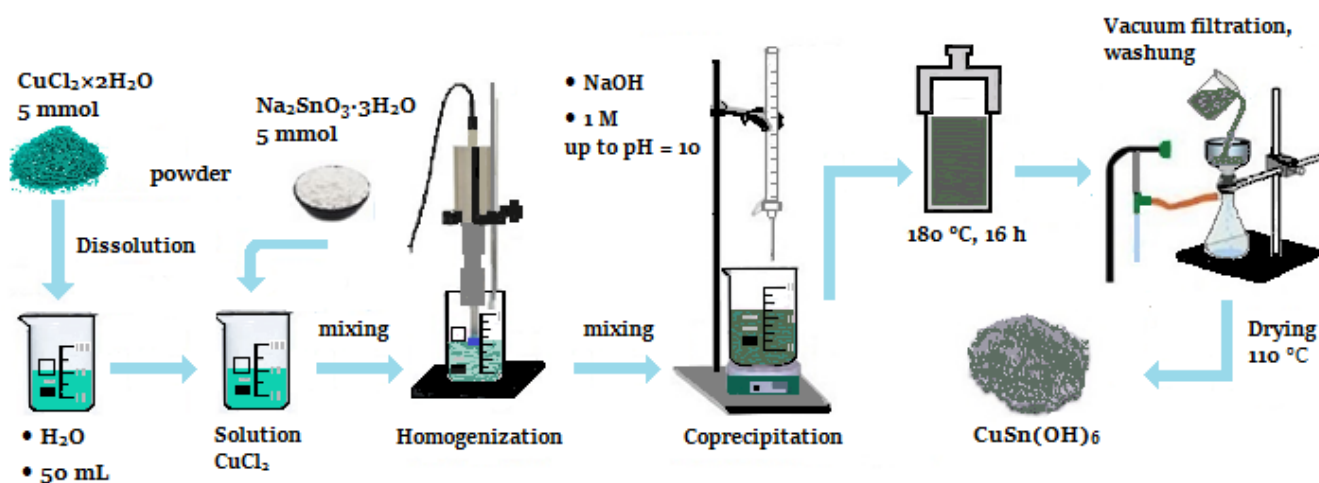


Figure 1 Sample preparation technique.

The microstructure of the samples was studied by field emission scanning electron microscopy (SEM) on a Hitachi SU8000 electron microscope. The images were taken in the secondary electron recording mode at an accelerating voltage of 2–30 kV and a working distance of 8–10 mm. The samples were analyzed by energy dispersive X-ray spectroscopy using an Oxford Instruments X-max energy dispersive spectrometer. The specific surface area was calculated from the analysis of low-temperature nitrogen adsorption isotherms at 77 K using the Brunauer-Emmett-Teller (BET) method on a Quantachrome Nova 1000e static instrument. Infrared spectra were recorded on a Carry 660 FTIR (Fourier transform infrared) spectrometer (Agilent Technologies, Santa Clara, CA, USA) with a PIKE Technologies Gladi ATR (diamond crystal) broken total internal reflection attachment in the range of 500–4000 cm^{-1} . The samples were prepared as vacuum-pressed KBr pellets with an admixture of the compound under study.

The analysis of the chemical composition of the samples to determine the concentration of tin and copper was carried out by the atomic emission spectrometry method using Agilent 7500A Inductively Coupled Plasma Spectrometer.

2.3. Testing of gas sensors

CuSn(OH)_6 and the product of its thermolysis (amorphous CuSnO_3) were used to fabricate the NO_2 gas sensor. The main problem was its low conductivity at room temperature that prevented the detection of response without heating. Therefore, the composites with the conductive additive were prepared. The carbon nanofibers (CNFs) with “fish-bone” structure, synthesized using CVD (Chemical vapor deposition) process using $\text{Ni/Al}_2\text{O}_3$ catalyst [43], were used as the additive for constructing the sensor. Specific surface area of CNFs was 110 m^2/g .

Composite films were fabricated using an aerosol spraying technique. This process involves the use of an airbrush to uniformly spray the suspension on the sensor substrate. For suspension preparation, 95% $\text{C}_2\text{H}_5\text{OH}$ was used as the solvent. The substrates consisting of polyimide film with a

copper foil were used for the deposition of thin film of 40% CuSn(OH)_6 /60%CNFs and 40% CuSnO_3 /60%CNFs (w/w) composite. The suspension, composed of carbon nanofibers (particle size <80 μm) and composite materials, was prepared via ultrasonic dispersion in 10 mL of ethanol. The dispersion process was carried out in an UZV3/200 ultrasonic bath (22 kHz, 85 W, 8.5 W/cm^3) for 20 min.

For the active layer formation, the suspension was spray-coated onto the substrate, which was preheated to 60 °C. The deposited film partially overlapped the copper contacts. The suspension of composite material with a concentration of 3 mg/mL was used for spraying.

The testing of gas sensors was carried out using the gas station with the gas supply lines for the carrier gas and analytes. The description of the gas station was fully given in [44]. Synthetic air (a mixture of 21 vol.% O_2 and 79 vol.% N_2) was used as the carrier gas. Nitrogen dioxide was used as the analyte (Passport F-48810, standard of gas mixture according to GSO 10599-2015; supplied by “PGS-Servis” Co. Ltd., Russia). The total flow rate of the gas mixture supplied to the measurement cell was 100 mL/min during the detection of nitrogen dioxide. The analyte concentration in the system was adjusted by regulating the flow rates from the gas cylinders. The specificity of sensors toward $\text{NO}_2/\text{N}_2\text{O}_4$ (two gases which are in equilibrium in a vessel) was not taken into account, assuming that sensor reacted to NO_2 adsorption at 25 °C.

The method for measuring gas-sensitive properties involved several stages. In the first stage, a baseline measurement was performed for 45 min, during which synthetic air was supplied at a rate of 100 mL/min. This was necessary to establish the initial resistance level (baseline). The baseline (response of air) was fitted using the linear function and then subtracted from the data recorded for the analyte. When, the analyte was introduced, the system was purged with air every 10 min. During the measurements, the gas sensor was placed inside the measurement chamber on a heater powered by a direct current source. To determine the sensor resistance, a two-electrode method was used,

and the measurements were conducted at room temperature (25 ± 2 °C). The volume of the chamber was 250 cm^3 . During the adsorption/desorption of the analyte, changes in the sensor resistance were observed. These changes were recorded using a Keithley 2401 source meter (Keithley Instruments, USA) with a voltage of 0.1 V using the two-contact technique. Data collection was performed using specialized software.

To evaluate the sensor response to the detected analyte, the relative sensor response was calculated as the ratio between the change in the sensor resistance (ΔR) during the experiment and the initial resistance of the sensor in air (R_0) using equation (2):

$$\Delta R/R_0 = ((R - R_0)/R_0) \cdot 100\%, \quad (2)$$

where R is the electrical resistance of the sensor during exposure to the analyzed gas, Ω ; R_0 is the initial electrical resistance when exposed to the carrier gas (air), Ω .

2.4 Electrochemical testing

The specific capacitance of the obtained composite materials was determined using the cyclic voltammetry method. The voltammetric curves were recorded using an Elins P-40X single-channel potentiostat/galvanostat («Electrochemical Instruments», Chernogolovka, Russia). A three-electrode scheme was used for the measurements. The auxiliary electrode was a platinum wire (Pt), and the reference electrode was a silver/silver chloride (Ag/AgCl, saturated KCl) one. The working electrode was a composite based on copper hydroxy- or stannate/modifier CNF).

The composite weighing about 0.01 g was uniformly applied in a thin layer onto a graphite current collector with a cross-sectional area of 1 cm^2 . For the preparation of composite material samples, a simple mixing method was used: 5 wt.% of the polymer binder, polyvinylidene fluoride (PVDF), was mixed with 35 wt.% of copper stannate and 60 wt.% of modified CNFs. The mixture was mechanically stirred and dried at 60 °C for 30 min to remove the solvent. The modified CNFs were obtained by chemical treatment in a 6 M HNO_3 solution for 6 h at 80 °C with constant stirring. The resulting material was filtered and thoroughly washed with hot distilled water until neutral pH was achieved. To determine nitrate ions in the samples, a 1% diphenylamine solution in concentrated sulfuric acid was used. The absence of blue color with diphenylamine indicated the absence of nitrate ions in the samples. The carbon precipitate on the filter was dried at 100 °C for 12 h.

The electrodes were immersed in a 1 M H_2SO_4 solution, and cyclic voltammetry curves were recorded by changing the potential on the working electrode from 0 to 1 V using direct voltammetry. The measurements were performed at a potential scan rate of 2 mV/s. The specific capacitance of the material was calculated based on the obtained voltammetric curves using the following equation [45]:

$$\Delta C_{sp} = I/(v \cdot m), \quad (3)$$

where C_{sp} is the specific capacitance, F/g; I is the sum of the cathode and anode currents ($I = I_{\text{cathodic}} + I_{\text{anodic}}$) at 500 mV, mA; m is the weight of material, g; v is the sweep rate, mV/s.

3. Results and Discussions

According to the X-ray diffraction, the pattern of the sample obtained via hydrothermal synthesis and dried at 110 °C in air (Figure 2, curve 1) shows reflections characteristic of copper hexahydroxostannate $\text{CuSn}(\text{OH})_6$, which has a crystal structure with a tetragonal unit cell (space group $P4_2/nnm$, PDF4, card no. 70-117). The most intense diffraction peaks of the sample, with angles around $2\theta = 19.85^\circ$, 21.92° , 23.42° , 32.3° , 40.3° , 47.92° , and 58.95° , correspond to the (111), (002), (200), (202), (222), (400), and (422) planes, respectively, which is consistent with literature data [36,46].

The unit cell parameters of the $\text{CuSn}(\text{OH})_6$ phase, calculated using the Rietveld method in the Powder Cell 2.4 software, were $a = b = 7.7560 \pm 0.0003 \text{ \AA}$ and $c = 8.0960 \pm 0.0005 \text{ \AA}$, which is close to the corresponding values previously calculated for this compound and reported in [46].

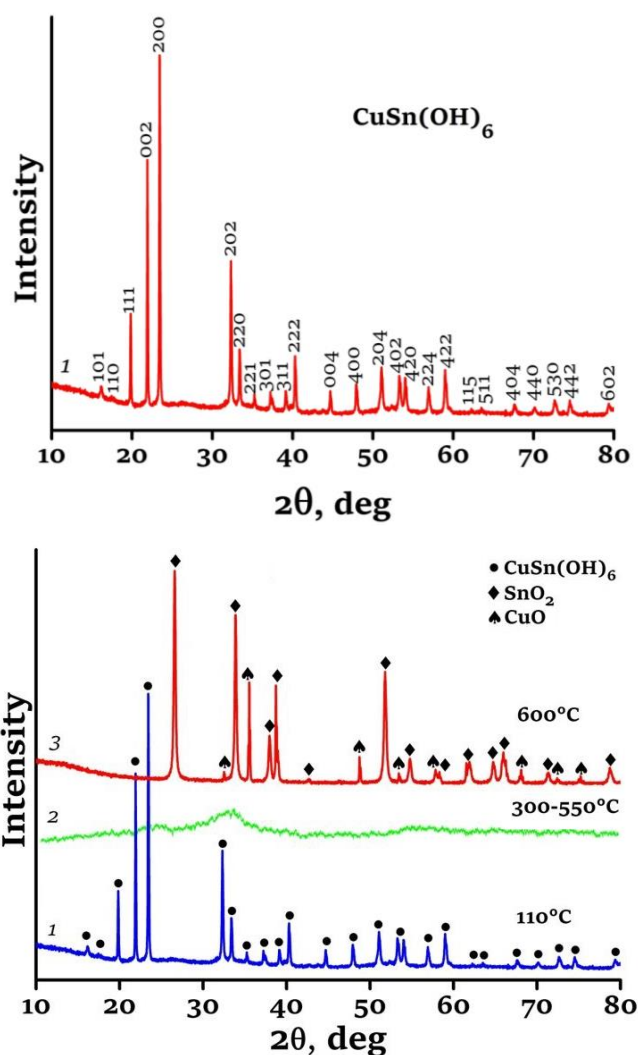
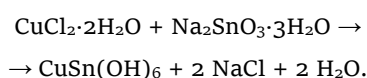


Figure 2 X-ray diffraction patterns of the freshly deposited $\text{CuSn}(\text{OH})_6$ sample (a) and thermolysis products obtained at temperatures of 300...550 °C (2) and 600 °C (3).

The average crystallite size of the sample, calculated by the Rietveld method, correlates with the size estimated by the Scherrer equation. The average nanoparticle size, calculated using the most intense peak (200) at $2\theta = 23.42^\circ$, was about 35–38 nm. According to atomic emission spectrometry, the mass fractions of copper and tin were $22.2 \pm 0.2\%$ (99.3% of the theoretical value) and $41.5 \pm 0.3\%$ (99.4% of the theoretical value), respectively, which corresponds to a Cu:Sn atomic ratio of 1:1. These data are consistent with the results obtained by energy-dispersive X-ray spectroscopy (EDX), according to which the atomic ratio Cu:Sn:O is in the range of $(9.5 \pm 0.5):(9.5 \pm 0.5):(57 \pm 3)$, which is close to the stoichiometric ratio for CuSn(OH)_6 .

Thus, the formation of CuSn(OH)_6 can be represented by the following scheme:



According to electron microscopy (Figure 3a), the CuSn(OH)_6 samples ($S = 41 \text{ m}^2/\text{g}$) are characterized by non-uniform cubic-shaped particles measuring 2–5 μm , along with the presence of agglomerates composed of these particles.

The crystallite size L , calculated from the specific surface area S_{sp} using a simplified expression for spherical or cubic particles, was 12–15 nm:

$$L \approx 6/(\rho \cdot S_{\text{sp}}), \quad (4)$$

where ρ is the density of substance (for CuSn(OH)_6 the X-ray density was $\rho = 7.586 \text{ g}\cdot\text{cm}^{-3}$; PDF4 card no. 70-117).

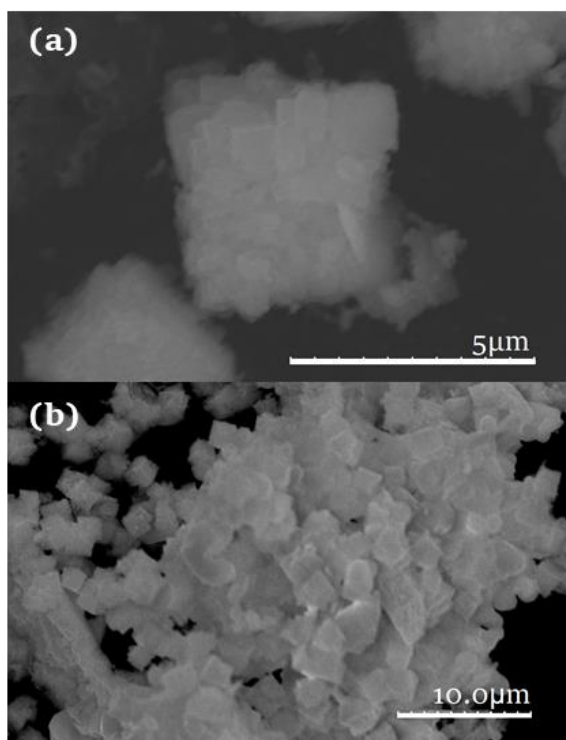
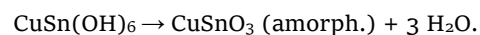


Figure 3 SEM images of the CuSn(OH)_6 sample (a) and of the product of its thermolysis (b).

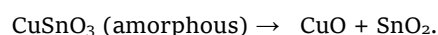
According to the thermal analysis data shown in Figure 4, the heating of CuSn(OH)_6 involves sequential processes accompanied by changes in mass, structure, and phase composition, which is consistent with the results of X-ray diffraction. When the sample is heated in the temperature range of 110–300 $^\circ\text{C}$, a mass loss of $\sim 18.85\%$ is observed, which quantitatively corresponds to the calculated value ($\sim 19.01\%$) for the reaction:



The reaction is accompanied with the endothermic effect at $T_{\text{max}} = 276 \text{ }^\circ\text{C}$ with the formation of amorphous CuSnO_3 ($S_{\text{sp}} = 65 \text{ m}^2/\text{g}$) (Figure 2, curve 2). Figure 3b shows that copper stannate possessed the same cube-like morphology as the precursor, CuSn(OH)_6 , but with the finer (1–3 μm) particle size.

From the analysis of TG-DTA curves, no obvious weight loss and endothermic (or exothermic) phenomenon were observed between 300 and 550 $^\circ\text{C}$, which shows that CuSnO_3 is stable under this temperature range. The further annealing at 550–600 $^\circ\text{C}$ led to appearance of exothermic effect caused by decomposition of amorphous phase of copper stannate with the formation of rutile-type SnO_2 phase (PDF4 database; card no. 77-477) and tenorite-type CuO (PDF4 database; card no. 72-629) (Figure 2, curve 3).

The following process of thermal decomposition can be represented by the following reaction:



The Fourier transform infrared spectrum of CuSn(OH)_6 (Figure 5, curve 1) showed the bands at 3125 and 3213 cm^{-1} , corresponding to the O–H stretching vibrations attributed to the presence of adsorbed water. The peak at 1157 cm^{-1} is due to the Sn–OH bending vibration, while the peaks at 765 cm^{-1} and 737 cm^{-1} are related to water-water hydrogen bonds. Furthermore, the peaks at 1393 cm^{-1} and 532 cm^{-1} are caused by Sn–O bond vibrations. In the absorption spectrum of CuSnO_3 (Figure 5, curve 2), bands are observed at 1385, 1111 cm^{-1} , and 522 cm^{-1} , which are characteristic of Sn–O and Cu–O bonds [36,39,46,47].

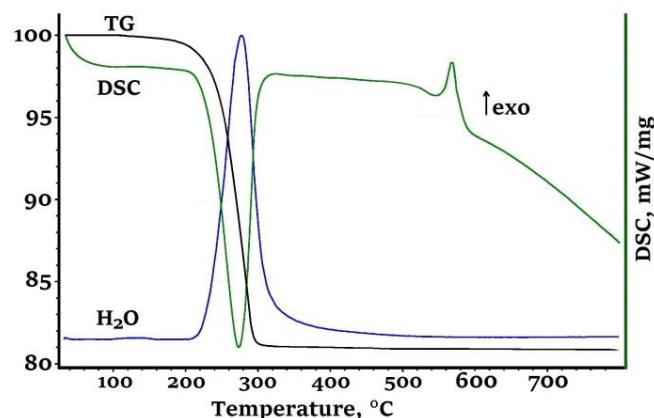


Figure 4 TG/DSC curves of the CuSn(OH)_6 sample.

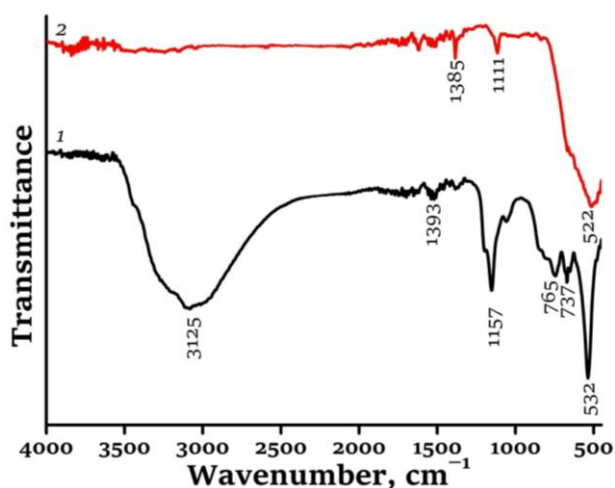


Figure 5 FTIR absorption spectrum of CuSn(OH)_6 (1) and the product of its thermolysis (amorphous CuSnO_3) (2).

Figure 6 shows the sensitivity curves of gas sensors to nitrogen dioxide at room temperature. It can be seen that the prepared composites demonstrated a high response to NO_2 at 25°C compared to pure CNFs (more than 10 times higher for $\text{CuSnO}_3/\text{modified CNFs}$ composite). All the sensors studied showed decrease in the sensor resistance in contact with NO_2 . The slope of the response curve depends on the adsorption mechanism. CNFs exhibit p-type semiconductor behavior (in terms of their interaction with NO_2), where the main charge carriers are holes, and the interaction with electron-acceptor gas (e.g., NO_2) leads to an increase in hole concentration in the material [48]. The composites based on copper stannate and copper hydroxystannate showed the same behavior, facilitating in a decrease in sensor resistance in contact with nitrogen dioxide.

Comparing the samples with each other, it can be said that the composite of CuSnO_3 and modified CNFs possessed the highest response (32% at 2 ppm) compared to the $\text{CuSn(OH)}_6/\text{modified CNFs}$ (19% at 2 ppm). These two stannate-containing systems played the role of heterogeneous additive to oxidized CNFs, forming the hole depletion regions on the surface of the sensing material [49]. The limit of detection $\text{LoD}=(3.3\cdot\sigma)/\mu$, demonstrates the decrease of LoD of $\text{CuSn(OH)}_6/\text{modified CNFs}$ system (13.0 ppm) compared to CNFs (619 ppb) or $\text{CuSn(OH)}_6/\text{modified CNFs}$ (9.7 ppm). This is mainly caused by high value of standard deviation (σ) related to sensitivity (μ). The composites showed significantly higher non-linearity and more than 10 times higher σ compared to CNFs, whereas the sensitivity of these samples ranged within 1.2–2.5%/ppm, and the latter contributed to a lesser degree to LoD values. The summary of sensor characteristics is given below (Table 1).

The response time of the composite based on CuSnO_3 and modified CNFs decreased by 25–33 s compared to the other samples. The recovery time τ_{recovery} estimated using the $R = y_0 + A \cdot (\exp(-t/\tau_{\text{recovery}}))$ equation [50] showed the faster recovery of the sensor compared to that of the CNFs.

Table 1 Characteristics of sensors.

Sample	LoD, ppm	Response time*, s	Recovery time*, min
CNFs (modified)	0.619	443	1007
$\text{CuSn(OH)}_6/\text{modified CNFs}$	9.7	435	831
$\text{CuSnO}_3/\text{modified CNFs}$	13.0	410	

* The values were calculated at 2 ppm adsorption cycle.

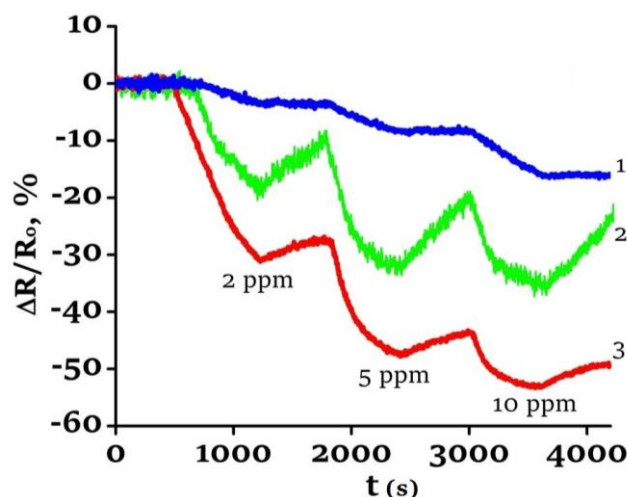


Figure 6 Sensor response to NO_2 at room temperature ($25 \pm 1^\circ\text{C}$): modified CNFs (1), $\text{CuSn(OH)}_6/\text{modified CNFs}$ (2), $\text{CuSnO}_3/\text{modified CNFs}$ composite (3).

The fact that copper stannate provides higher response than copper hydroxystannate is probably caused by the different morphology and crystal state (amorphous or crystalline).

Figure 7(a, b) shows the cyclic voltammetry curves at 2 mV/s sweep rate for the samples obtained by hydrothermal technique (a) and annealed at 400°C (b). At it can be seen from curves 1 in Figure 7, the electrochemical activity of pristine samples was low. Low current density values obtained within the potential windows were obtained that is cause with insufficient electron conductivity. Table 2 shows the specific capacitance.

As it was reported in [30–32, 51], one of the effective approaches to enhancing the conductivity of functional materials is the creation of composites based on modified CNFs. In order to estimate the impact of CNFs, a comparison of electrochemical behavior of composites with pure stannates and modified CNFs was carried out. It was found that the addition of modified CNFs with hydroxystannate and copper stannate led to considerable growth in current density within the potential window (Figure 7a,b, curves 2 and 3).

Table 2 Specific capacitance of the samples (at 2 mV/s; 1M H_2SO_4).

Sample	Specific capacitance, F/g
CuSn(OH)_6	6
CuSnO_3	14
CNFs (modified)	83
$\text{CuSn(OH)}_6/\text{modified CNFs}$	135
$\text{CuSnO}_3/\text{modified CNFs}$	288

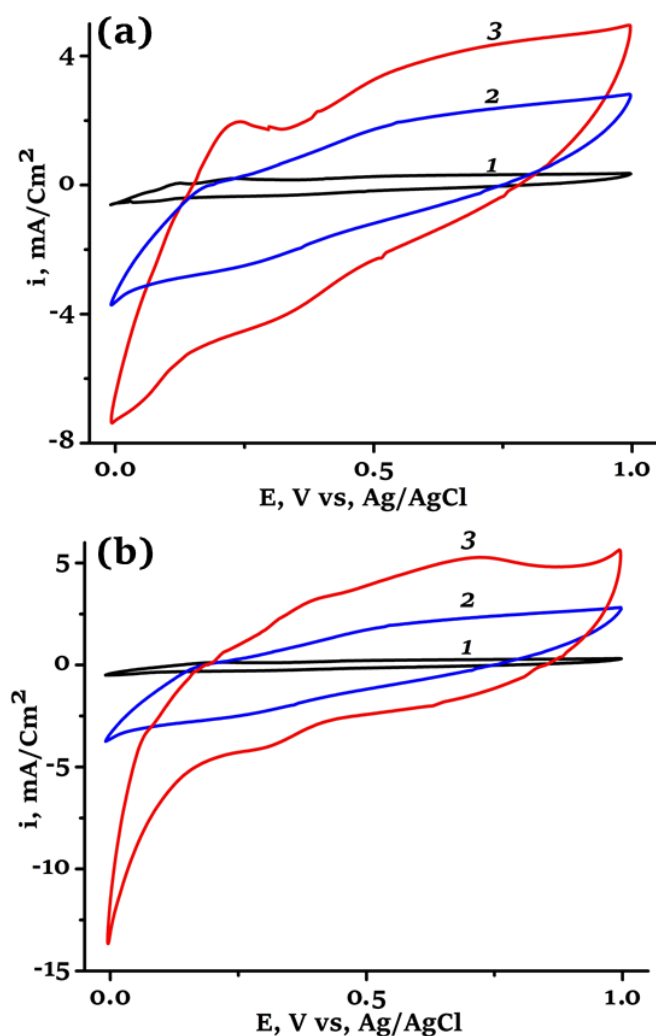


Figure 7 Cyclic voltammetry curves measured on electrodes made of: (a) 1 - hydroxostannate $\text{CuSn}(\text{OH})_6$, 2 - modified CNFs, 3 - $\text{CuSn}(\text{OH})_6$ /modified CNFs; (b) 1 - copper stannate CuSnO_3 , 2 - modified CNFs, 3 - CuSnO_3 /modified CNFs.

Analysis of voltammetry curves (Figure 7) makes it possible to conclude that specific capacitance of composite is determined not only by the presence of modified CNFs, but also by the nature of electrochemically active material. It was pointed out by the fact that the copper stannate electrodes demonstrated higher specific capacitance than the hydroxostannate ones. The observed difference electrochemical characteristics are probably caused by the particle morphology. It can be proposed that the synthesis of copper hydroxostannate led to the formation of the larger size of particles compared to copper stannate. The higher surface area of the material based on CuSnO_3 in turn provides the number of active sites for passing the Faradaic reactions and enhances the availability for sulfuric acid electrolyte, increasing the total capacitance of the composites.

4. Limitations

This work shows the possibility for using the composites based on modified CNFs and either copper hydroxostannate or copper stannate as a sensitive element for gas sensors

and an electrode material for energy storage devices. The main problem is the low conductivity of the stannates at room temperature. Application of CNFs makes it possible to improve not only the conductivity of the sensing material, but also to enhance the other electrochemical properties, crucial for the electrodes for electrochemical devices, e.g., supercapacitors. This issue should be studied to improve the characteristics.

5. Conclusions

This work demonstrates that the perovskite-like copper hydroxostannate forms as a result of hydrothermal synthesis at 180 °C for 16 h and consists of cubic particles measuring 2–5 μm with a specific surface area of 41 m^2/g . It is shown that upon thermolysis of $\text{CuSn}(\text{OH})_6$ above 300 °C, an amorphous and thermally stable up to 500 °C copper stannate CuSnO_3 is produced. Further temperature increase (above 550 °C) results in an exothermic effect due to the decomposition of CuSnO_3 with the formation of tin(IV) oxide and copper(II) oxide. The reaction of the CuSnO_3 /modified CNFs composite with NO_2 at room temperature reaches 32% response at 2 ppm, while the response of the $\text{CuSn}(\text{OH})_6$ /modified CNFs composite under the same conditions is 19%. The CuSnO_3 /modified CNFs composite material demonstrates its potential application as an electrode material in supercapacitors, showing a specific capacitance of 288 F/g compared to 135 F/g for the $\text{CuSn}(\text{OH})_6$ /modified CNFs composite. The specific capacitance of the composites based on CNFs significantly exceeds that of single-phase hydroxostannates and copper stannates (14 and 6 F/g, respectively). Thus, the CuSnO_3 /modified CNFs composite is a promising material not only for room-temperature NO_2 gas sensors but also for energy storage systems.

Supplementary materials

No supplementary materials are available.

Data availability statement

The datasets used and/or analyzed during the current study available from the corresponding author on reasonable request.

Acknowledgments

None.

Author contributions

Conceptualization: A.V.L., A.I.A., O.N.N., A.G.B.
 Data curation: A.I.A.
 Formal Analysis: A.I.A., O.N.N., A.G.B.
 Funding acquisition: A.G.B.
 Investigation: A.I.A., O.N.N., A.G.B., A.V.L.
 Methodology: A.I.A., O.N.N., A.G.B.
 Project administration: A.I.A., A.G.B.
 Resources: A.G.B.
 Software: A.V.L., O.N.N.
 Supervision: A.G.B.
 Validation: A.I.A., A.G.B., A.V.L.
 Visualization: A.I.A., O.N.N., A.G.B., A.V.L.
 Writing – original draft: A.I.A., A.V.L.
 Writing – review & editing: A.G.B.

Conflict of interest

The authors declare no conflict of interest.

Additional information

Author IDs:

Anton V. Loginov, Scopus ID [57189525710](#);
Alexander I. Aparnev Scopus ID [7801309186](#);
Oksana N. Novgorodtseva, Scopus ID [57215185765](#);
Alexander G. Bannov, Scopus ID [54788777600](#);

Website:

Novosibirsk State Technical University, <https://en.nstu.ru/>.

References

- Yuan F, Ma S, Wen Y, Liu W, Pei S, Wang S, Zhang Q. The impact of Zn vacancy on gas sensitivity of ZnSn(OH)₆. *Appl Surface Sci.* 2022;614:1560. doi:[10.1016/j.apsusc.2022.156058](#)
- Guo W, Li X, Gao X, Zeng W, Wang X. Designed synthesis of Fe-doped CoSn(OH)₆ nanocubes with enhanced N-butyl alcohol gas sensing properties. *Sensors Actuators B Chem.* 2023;379: 133292. doi:[10.1016/j.snb.2023.133292](#)
- Loginov AV, Aparnev AI, Bannov AG. Synthesis of copper-doped nanocrystalline tin stannate by thermal decomposition of a precursor. *Chimica Techno Acta.* 2024;11(4):202411405. doi:[10.15826/chimtech.2024.11.4.05](#)
- Yan B, Lin L, Sun H, Zhang T, Xu C, Sun C, Zhang L, Yang X. Double-shelled NiS/SnS@N-doped carbon nanoboxes engineered from NiSn(OH)₆ cube templates for advanced sodium-ion battery anodes. *Chem Engin J.* 2023;477:146950. doi:[10.1016/j.cej.2023.146950](#)
- Mandal M, Chattopadhyay K, Chakraborty M, Shin W, Bera KK, Chatterjee S, Hossain A, Majumdar D, Gayen A, Nah C, Bhattacharya SK. Room Temperature Synthesis of Perovskite Hydroxide, MnSn(OH)₆: A Negative Electrode for Supercapacitor. *Electronic Mater Lett.* 2022;18:559-567. doi:[10.1007/s13391-022-00366-4](#)
- Li B., Zhang GX, Huang KS, Qiao LF, Pang H. One-step synthesis of CoSn(OH)₆ nanocubes for high-performance all solid-state flexible supercapacitors. *Rare Met.* 2017;36(5):457-464. doi:[10.1007/s12598-017-0890-0](#)
- Hu X, Tang Y, Xiao T, Jiang J, Jia Z, Li D, Li B, Luo L. Rapid Synthesis of single-crystalline SrSn(OH)₆ nanowires and the performance of SrSnO₃ nanorods used as anode materials for Li-ion battery. *J Phys Chem C.* 2010;114(2):947-952. doi:[10.1021/jp909903k](#)
- Rani BJ, Yuvakkumar R, Ravi G, Kumar P, Babu ES, Saravanakumar B, Velauthapillai D. High performance MnSn(OH)₆ electrodes for energy conversion application. *Mater Lett.* 2021;282:128888. doi:[10.1016/j.matlet.2020.128888](#)
- Velmurugan G, Raman RG, Prakash D, Kim I, Sahadevan J, Sivaprakash P. Influence of Ni and Sn Perovskite NiSn(OH)₆ Nanoparticles on Energy Storage Applications. *Nanomater.* 2023;13:1523. doi:[10.3390/nano13091523](#)
- Isacfranklin M, Rani BJ, Kumar PS, Yuvakkumar GR, Ravi A, Manigandan M, Thambidurai, Dang C, Velauthapillai D. Electrochemical energy storage and conversion applications of CoSn(OH)₆ materials. *Int J Hydrog Energy.* 2022;47(100):41948-41955. doi:[10.1016/j.ijhydene.2021.08.001](#)
- Nagajyothi PC, Tettey CO, Ramaraghavulu R, Bhargava A, Siddiqui MR, Dillip GR, Shim J. Tailoring the composition of a non-noble, Cubic Shaped MnSn(OH)₆ Bi-functional electrocatalysts for methanol and urea oxidation reactions in alkaline solutions. *Surfaces Interfaces.* 2024;51:104712. doi:[10.1016/j.surfin.2024.104712](#)
- Huang D, Fu X, Long J, Jiang X, Chang L, Meng S, Chen S. Hydrothermal synthesis of MSn(OH)₆ (M=Co, Cu, Fe, Mg, Mn, Zn) and their photocatalytic activity for the destruction of gaseous benzene. *Chem Engin J.* 2015;269:168-179. doi:[10.1016/j.cej.2015.01.133](#)
- Yanpei L, Jing C, Jiawen L, Yu S, Xiaofang L, Danzhen L. Hydroxide SrSn(OH)₆: A new photocatalyst for degradation of benzene and rhodamine B. *Appl Catal B.* 2016;182:533-540. doi:[10.1016/j.apcatb.2015.09.051](#)
- Sun M, Yang B, Yan J, Zhou Y, Huang Z, Zhang N, Mo R, Ma R. Perovskite CoSn(OH)₆ nanocubes with tuned d-band states towards enhanced oxygen evolution reactions. *Nanoscale.* 2024;16:10618-10627. doi:[10.1039/D4NR00975D](#)
- Li Y, Pu H, Hong C, Gong X, Chen Y, Zhang Y, Qian H, Gao J, Wan C, Yang D. CoSn(OH)₆ nanocubes: Hydroxyl perovskite catalyst for efficient peroxy monosulfate activation in acetamiprid degradation. *Environ Res.* 2025;272:121149. doi:[10.1016/j.envres.2025.121149](#)
- Fang Y, Fang Y, Zong R, Yu Z, Tao Y, Shao J. In situ surface reconstruction of a Ni-based perovskite hydroxide catalyst for an efficient oxygen evolution reaction. *J Mater Chem A.* 2022;10:1369. doi:[10.1039/d1ta08531j](#)
- Wang X, Zhou X, Jin R, Tan T, Ma H, Fang R, Deng B, Dong F. Defect-poor BaSn(OH)₆ enhanced charge separation for efficient photocatalytic degradation of toluene. *J Environ Sci.* 2023;134:86-95. doi:[10.1016/j.jes.2022.10.036](#)
- Sandesh S, Kumar RP, Kristachar, PM, Halgeri AB, Ganapati VS. Synthesis of biodiesel and acetins by transesterification reactions using novel CaSn(OH)₆ heterogeneous base catalyst. *Appl Catalysis A General.* 2016;523:1-11. doi:[10.1016/j.apcata.2016.05.006](#)
- Zhao Y, Kumar ST, Ghanem MA, Reddy GR, Joo SW. Nanocube-structured ZnSn(OH)₆ for enhanced bifunctional electrocatalysis in oxygen evolution and urea oxidation reactions. *Solid State Ionics.* 2025;427:116915. doi:[10.1016/j.ssi.2025.116915](#)
- Hu X, Lv G, Jia Z, Jiang J, Xiao T, Yuan M, Tang Y. A General Sonochemical Approach to Rapid Synthesis of 1D Single-Crystalline MSn(OH)₆ (M = Ba, Ca, Sr) Nanostructures. *Appl Surf Sci.* 2011;257(21): 9008-9013. doi:[10.1016/j.apsusc.2011.05.088](#)
- Kramer JW, Kelly B, Manivannan V. Synthesis of MSn(OH)₆ (where M = Mg, Ca, Zn, Mn, or Cu) materials at room temperature. *Cent Eur J Chem.* 2010;8(1):65-69. doi:[10.2478/s11532-009-0094-z](#)
- Jena H, Kutty KVG, Kutty TRN. Ionic transport and structural investigations on MSn(OH)₆ (M = Ba, Ca, Mg, Co, Zn, Fe, Mn) hydroxide perovskites synthesized by wet sonochemical methods. *Mater Chem Phys.* 2004;88:167-179. doi:[10.1016/j.matchemphys.2004.07.003](#)
- Mizoguchi H, Bhuvanesh NSP, Kim Y, Ohara S, Woodward PM. Hydrothermal Crystal Growth and Structure Determination of Double Hydroxides LiSb(OH)₆, BaSn(OH)₆, and SrSn(OH)₆. *Inorg Chem.* 2014;53(19):10570-10577. doi:[10.1021/ic5016252](#)
- Sahoo S, Sood A, Kumar R, Milton A, Choi SM, Jo YJ, Hussain I, Han SS. Rapid in-situ fabrication of MnSnO₃ perovskite-based nanocomposites via microwave-assisted approach for supercapacitor devices. *J Energy Storage.* 2025;110:115368. doi:[10.1016/j.est.2025.115368](#)
- Gaudon M, Salek G, Kande M, Andron I, Frayret C, Durand E, Penin N, Duttine M, Wattiaux A, Jubera V. CaSn(OH)₆ hydroxides, CaSnO₃ oxides and CaSnF₆ fluorides: Synthesis and structural filiation. Cationic environment impact on Pr³⁺ doped compounds luminescence. *J Solid State Chem.* 2018;265:291-298. doi:[10.1016/j.jssc.2018.06.017](#)
- Loginov AV, Aparnev AI, Uvarov NF. Nanocomposites prepared via thermal decomposition of calcium hydroxystannate CaSn(OH)₆. *Inorg Mater.* 2022;58(8):814-821. doi:[10.1134/S0020168522080088](#)
- Manikanta P, Mohanty J, Mounesh, Rohit RN, Sandeep S, Santhosh AS, Pramoda K, Bhari MN. Recent advances and current status of semiconductor stannate-based electrode materials for electrochemical sensing and energy

- applications. *J Alloys Compd.* 2025;1020:179370. doi:[10.1016/j.jallcom.2025.179370](https://doi.org/10.1016/j.jallcom.2025.179370)
28. Swati S, Prakash C. Supercapacitor and electrochemical techniques: A brief review. *Res Chem.* 2023;5:100885. doi:[10.1016/j.rechem.2023.100885](https://doi.org/10.1016/j.rechem.2023.100885)
29. Kumar N, Kim S-B, Lee S-Y, Park S-J. Recent Advanced Supercapacitor: A Review of Storage Mechanisms, Electrode Materials, Modification, and Perspectives. *Nanomater.* 2022;12(20):3708. doi:[10.3390/nano12203708](https://doi.org/10.3390/nano12203708)
30. Saranya PE, Selladurai S. Facile synthesis of NiSnO₃/graphene nanocomposite for high-performance electrode towards asymmetric supercapacitor device. *J Mater Sci.* 2018;53:16022–16046. doi:[10.1007/s10853-018-2742-1](https://doi.org/10.1007/s10853-018-2742-1)
31. Abid MH, Alharbi FF, Gassoumi A, Aslam M. FeSnO₃/rGO nanocomposite electrode development for supercapacitor application. *J Alloys Compd.* 2024;1008:176632. doi:[10.1016/j.jallcom.2024.176632](https://doi.org/10.1016/j.jallcom.2024.176632)
32. Wang G, Sun X, Lu F, Yu Q, Liu C, Lian J. Controlled synthesis of MnSn(OH)₆/graphene nanocomposites and their electrochemical properties as capacitive materials. *J Solid State Chem.* 2012;185:172–179. doi:[10.1016/j.jssc.2011.11.015](https://doi.org/10.1016/j.jssc.2011.11.015)
33. Khalil HF, Yousef TA, Dakhil AA, Ferjani H, Alosaimi AM, Hameed RA, Afify N, El-Batouti M, Rayan DA, Kamoun EA, El-sharkawy SG. Nickel-Substituted CdSnO₃ Perovskite Nanoparticles: A New Frontier in Energy Storage. *J Electronic Mater.* 2025;54:6492–6505. doi:[10.1007/s11664-025-12071-7](https://doi.org/10.1007/s11664-025-12071-7)
34. Zhou Z, Chen T, Deng J, Yao Q, Wang Z, Zhou H. CuSn(OH)₆ nanocubes as high-performance anode materials for lithium-ion batteries. *Int J Electrochem Sci.* 2018;13:2001–2009. doi:[10.20964/2018.02.72](https://doi.org/10.20964/2018.02.72)
35. Mohanta D, Raha S, Gupta SV, Ahmaruzzaman Md. Bioinspired green synthesis of engineered CuSnO₃ quantum dots: An effective material for superior photocatalytic degradation of Rabeprazole. *Mater Lett.* 2019;240:193–196. doi:[10.1016/j.matlet.2018.12.104](https://doi.org/10.1016/j.matlet.2018.12.104)
36. Almahri A. Fenton-like photocatalytic degradation of Rhodamine 6G and tetracycline under sunlight irradiation using hexahydroxy copper-stannate CuSn(OH)₆. *Inorganic Chemistry Communications.* 2025;177:114340. doi:[10.1016/j.inoche.2025.114340](https://doi.org/10.1016/j.inoche.2025.114340)
37. Liua Y, Zhang J, Cui S, Wei H, Yang D. Perovskite hydroxide-based laccase mimics with controllable activity for environmental remediation and biosensing. *Biosensors Bioelectronics.* 2024;256:116275. doi:[10.1016/j.bios.2024.116275](https://doi.org/10.1016/j.bios.2024.116275)
38. Gnanamoorthy G, Yadav VK, Narayanan V. Well organized assembly of (X)- CuSnO₃ nanoparticles enhanced photocatalytic and anti-bacterial properties. *J Water Process Engin.* 2020;36:101258. doi:[10.1016/j.jwpe.2020.101258](https://doi.org/10.1016/j.jwpe.2020.101258)
39. Zhong S-L, Xu R, Wang L, Li Y, Zhang L-F. CuSn(OH)₆ submicrospheres: Room-temperature synthesis, growth mechanism, and weak antiferromagnetic behavior. *Mater Res Bull.* 2011;46(12):2385–2391. doi:[10.1016/j.materresbull.2011.08.053](https://doi.org/10.1016/j.materresbull.2011.08.053)
40. Xu R, Deng B, Min L, Xu H, Zhong S. CuSn(OH)₆ submicrospheres: Room-temperature synthesis and weak antiferromagnetic behavior. *Mater Lett.* 2011;65(4):733–735. doi:[10.1016/j.matlet.2010.11.061](https://doi.org/10.1016/j.matlet.2010.11.061)
41. Liu T, Du R, Kong X. Preparation and Electrochemical Properties of Amorphous Tin-copper composite Oxide CuSnO₃. *Adv Mater Res Vols.* 2012;535–537:31–35. doi:[10.4028/www.scientific.net/AMR.535-537.31](https://doi.org/10.4028/www.scientific.net/AMR.535-537.31)
42. Saranya PE, Selladurai S. Facile synthesis of NiSnO₃/graphene nanocomposite for high-performance electrode towards asymmetric supercapacitor device. *J Mater Sci.* 2018;53:16022–16046. doi:[10.1007/s10853-018-2742-1](https://doi.org/10.1007/s10853-018-2742-1)
43. Ermakova MA, Ermakov DY, Chuvilin AL, Kuvshinov GG. Decomposition of methane over iron catalysts at the range of moderate temperatures: The influence of structure of the catalytic systems and the reaction conditions on the yield of carbon and morphology of carbon filaments. *J Catal.* 2001;201:183–197. doi:[10.1006/jcat.2001.3243](https://doi.org/10.1006/jcat.2001.3243)
44. Lapekin NI, Kurmashov PB, Larina TV, Chesalov YA, Kurdyumov DS, Ukhina AV, Maksimovskiy EA, Ishchenko AV, Sysoev VI, Bannov AG. Carbon nanofibers synthesized at different pressures for detection of NO₂ at room temperature. *Chemosensors.* 2023;11(7):381. doi:[10.3390/chemosensors11070381](https://doi.org/10.3390/chemosensors11070381)
45. Shukla AK, Banerjee A, Ravikumar MK, Jalajakshi A. Electrochemical capacitors: Technical challenges and prognosis for future Markets. *Electrochim Acta.* 2012;84:165–173. doi:[10.1016/j.electacta.2012.03.059](https://doi.org/10.1016/j.electacta.2012.03.059)
46. Dong S, Cui L, Zhao Y, Wu Y, Xia L, Su X, Zhang C, Wang D, Guo W, Sun J. Crystal structure and photocatalytic properties of perovskite MSn(OH)₆ (M = Cu and Zn) composites with d¹⁰-d¹⁰ configuration. *Appl Surf Sci.* 2019;463:659–667. doi:[10.1016/j.apsusc.2018.09.006](https://doi.org/10.1016/j.apsusc.2018.09.006)
47. Babu BM, Sivakumar R, Sanjeeviraja C. Studies on the properties of copper tin hydroxidebased catalysts prepared by co-precipitation method for photocatalytic degradation of methylene blue dye. *J Mater Sci Mater Electron.* 2022;33:11687–11700. doi:[10.1007/s10854-022-08135-7](https://doi.org/10.1007/s10854-022-08135-7)
48. Chu SY, Wu MJ, Yeh TH, Lee CTing, Lee HY. Sensing Mechanism and Characterization of NO₂ Gas Sensors Using Gold-Black NP-Decorated Ga₂O₃ Nanorod Sensing Membranes. *ACS Sens.* 2024;9(1):118–125. doi:[10.1021/acssensors.3c01742](https://doi.org/10.1021/acssensors.3c01742)
49. Wang S, Yu H, Ge S, Wang Y, Gao C, Yu J. Insights into Chemical Bonds for Eliminating the Depletion Region and Accelerating the Photo-Induced Charge Efficient Separation toward Ultrasensitive Photoelectrochemical Sensing. *Biosensors.* 2023;13(11):984. doi:[10.3390/bios13110984](https://doi.org/10.3390/bios13110984)
50. Du H, Xie G, Su Y, Tai H, Du X, Yu H, Zhang Q. A New Model and Its Application for the Dynamic Response of RGO Resistive Gas Sensor. *Sensors.* 2019;19(4):889. doi:[10.3390/s19040889](https://doi.org/10.3390/s19040889)
51. Brester AE, Golovakhin VV, Novgorodtseva ON, Lapekin NI, Shestakov AA, Popov MV, Bannov AG. Chemically treated carbon nanofiber materials for supercapacitors. *Dokl Chem.* 2021;501(2):264–269. doi:[10.1134/S0012500821120016](https://doi.org/10.1134/S0012500821120016)